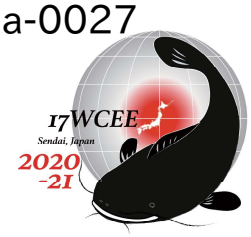

17th World Conference on Earthquake Engineering, 17WCEE
Sendai, Japan - September 27th to October 2nd, 2021

STRUCTURAL ASSESSMENT AND SPATIAL DAMPING IDENTIFICATION USING LOW-COST ACCELERATION SENSORS

H. Hummel[(1)], C. Málaga-Chuquitaype[(2)], T. Lee-Lewis[(3)] , N. Nanos [(4)]

[(1)] *MSc Student, Imperial College London, London, United Kingdom, heinrich.hummel17@imperial.ac.uk*
[(2)] *Senior Lecturer, Imperial College London, London, United Kingdom, c.malaga@imperial.ac.uk*
[(3)] *PhD Researcher, University of Portsmouth, Portsmouth, United Kingdom, timothy.lee-lewis@port.ac.uk*
[(4)] *Senior Lecturer, University of Portsmouth, Portsmouth, United Kingdom, nikos.nanos@port.ac.uk*

Abstract

The proper characterization of structural damping is one of the most current and challenging topics in mechanics, as damping has multiple sources and available theories are limited in their scope and explanatory power. At the same time, Microelectromechanical systems (MEMS) accelerometers are making inroads in low cost structural health monitoring applications and the available literature on the construction and use of open-source accelerometers is vast with many examples of sensing units built with low-cost electronic boards being published regularly. This paper presents a study on the structural characterization and damage identification of a model structure using low-cost wireless accelerometers built with of-the-shelf components. Natural frequencies, damping ratios, damping and stiffness matrices obtained from system output vectors by means of output-only modal identification (OMA) and a covariance driven stochastic subspace identification algorithms are presented together with an experimental modal identification (EMA) of viscous and hysteretic damping matrices. These methods are applied to a reduced physical model of a 2D steel frame and to its Finite Element (FE) representation. It is shown that, while the OMA method shows a good accuracy and stability for the FE data, it can yield unphysical results for the estimation of modal shapes and damping ratios during physical testing and often requires a significant user involvement. On the other hand, the EMA method shows high accuracy and stability as well as an improved potential for automatization. The model structure was then altered to simulated progressive states of damage (i.e. beam and column sections were reduced in both models, and bolted connections were loosened). Under these conditions, the natural frequencies dropped between 0.1 % and 22 % due to bolt loosening and between 0.8 % and 25.2% after beam and column section reductions. Overall, this paper shows that the localization of damage from low-cost wireless MEMS accelerometer data is possible on the basis of an integrated use of estimated stiffness, viscous and hysteretic damping matrices provided that reasonably low error levels are guaranteed.

Keywords: Low-cost sensing; MEMS accelerometers; vibration sensing; spatial damping identification; damage assessment

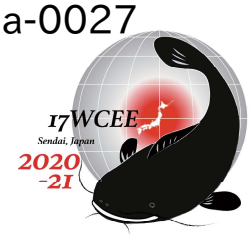

1. Introduction

Microelectromechanical systems (MEMS) accelerometers are making inroads in low cost structural health monitoring applications and the available literature on the construction and use of open-source accelerometers is vast with many examples of individual sensor units built with low-cost electronic boards published to date e.g. [1-4]. A good number of recent applications assume that the underlying hardware is behaving according to specification, and it is common practice to inherently trust the sensor output after some rudimentary validation and calibration procedures. Likewise, a minority of these implementations still uses cabled networks that are known to be prone to interference and reduce the quality of the output data in realistic scenarios [1]. However, MEMS technology for SHM also presents some advantages in terms of low cost, reduced size, limited weight, local interrogation, and small power consumption. Therefore, many studies have aimed at providing evidence of a close agreement between data obtained from low-cost wireless sensors e.g. [5] and data coming from commercially available devices e.g. [6].

In this context, the first motivation for this study is the need to test the applicability of in-house low-cost vibration sensors for the identification of a relatively elusive yet important structural engineering parameter: damping. Besides technical specifications like sensitivity, frequency bandwidth or noise; sensor costs play an important role in the decision-making process for a structure's inspection [7]. Fig. 1 shows a price comparison of tri-axial wireless vibration sensors regularly used in SHM, based on data from [7-9]. Because multiple sensors are required, on top of the hardware costs, data analysis and site labour; a full instrumentation campaign is expensive. The vibration sensors developed and employed in this study can be bought and assembled for less than $50 per unit, allowing the inspector to increase the number of measuring points, leading to a higher resolution of data.

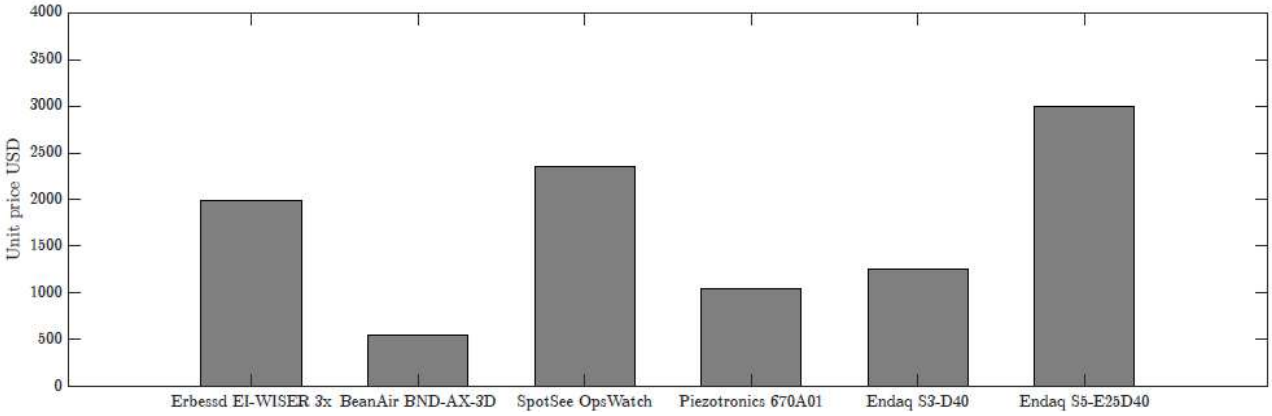

Fig. 1 – Price comparison of tri-axial vibration sensors for SHM

The structural state and damage after a strong earthquake can be investigated by evaluating the stiffness and the damping matrices of the structure of interest. However, typical numerical models used to simulate the damping behaviour of structures assume many simplifications of varying degree of approximation to the real behaviour. A rigorous simulation of damping in particular, remains one of the most challenging topics in engineering mechanics. Besides, for a good understanding of civil infrastructure, experimental confirmation of damping is crucial, and it constitutes a suitable limit test for the capabilities of the low-cost vibration-based monitoring system presented here. To this end, two types of modal analysis are employed herein: i) input-output or experimental modal analysis (EMA) where the loads from the excitation source are known, which can be achieved on site by placing geophones to capture the motion at the base, and ii) output-only modal analysis (OMA) with an ambient excitation considered as a zero mean Gaussian white noise and where estimates of the modal model are made only on the basis of the recorded output data (during or after the event).

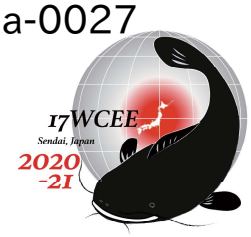

In both cases, modal parameters only draw a global picture of the dynamic behaviour. The stiffness and damping matrices are relevant to the behaviour of individual elements or parts of the structure and can provide key information for a preliminary damage localization. While inertia and stiffness contributions can be derived from first principles, damping ratios cannot and therefore require dynamic sensing. [10].

2. Structural model and experimental set-up

To carry out this study, an experimental model was built and tested at the Structures Laboratory of the University of Portsmouth. The physical frame is made of two 1600 mm tall EN8 type steel columns and a rectangular section of 25x3 mm. Each beam has a length of 396 mm and a rectangular section of 30x10 mm, made from S275 type steel. The beams are connected to the columns with bolted connections. The frame was bolted to a 1000x500x8 mm steel base plate. Fig. 2 shows a schematic view of the structure under consideration. Two loading conditions were considered: i) the unloaded structure with self-weight only and ii) the loaded structure with an added weight of 20N per level. A Finite Element Model (FEM) was constructed in OpenSees [11] to simulate the experimental specimen.

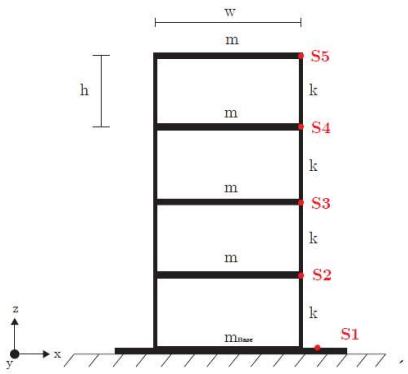

Fig. 2 – Schematic view of the 4-storey frame under study

A low-cost tri-axial accelerometer of the type ADXL355 was mounted on the base plate and on each level. Fig. 2 shows the sensor positions S1, ..., S5. The local sensor (x, y, z) axes coincide with the global (x, y, z) axes shown in Fig. 2. On each sensing node, a microcontroller of the type MCU MKR1000 was added to transfer the recorded data wirelessly. The data was then saved including a timestamp, sensor tag, and acceleration readings. (See Fig. 3). The sample frequency used was 100 Hz and the sensor accuracy level was set to 8g = 64000 counts.

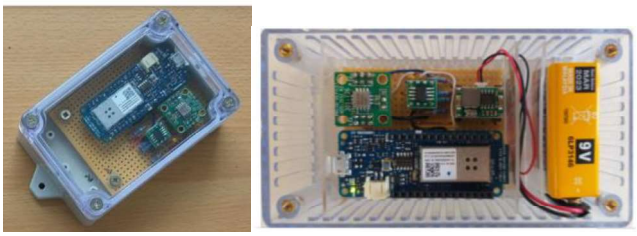

Fig. 3 – Low-cost wireless MEMS sensing unit

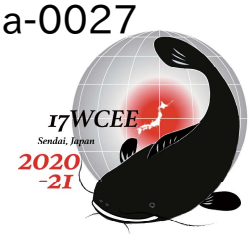

The lateral motion was simulated by means of an impact hammer installed at a height of 40mm above the fixed base. High-speed video footage was used to trach the motion of the hammer and determine its velocity. The transient load was modelled as a nearly rectangular pulse load of 10ms duration and 49.8N magnitude in the FEM.

3. Testing procedure and data processing

For each undamaged and damaged case, three impact tests were carried out consecutively with ambient vibration measurement taken before and after each test. The duration of each test was approx. 80s with the acceleration data recorded synchronized via cross-correlation and detrended. Subsequently, the acceleration histories were integrated twice to obtain displacements. A 9th order Butterworth bandpass filter was used to remove the DC bias. The upper and lower limits were adjusted for each test but stayed in the range of 1 Hz to 12 Hz. Fig. 4 shows the spectrograms obtained from the experiment together and with the OpenSees FEM model over a time period of 60 s.

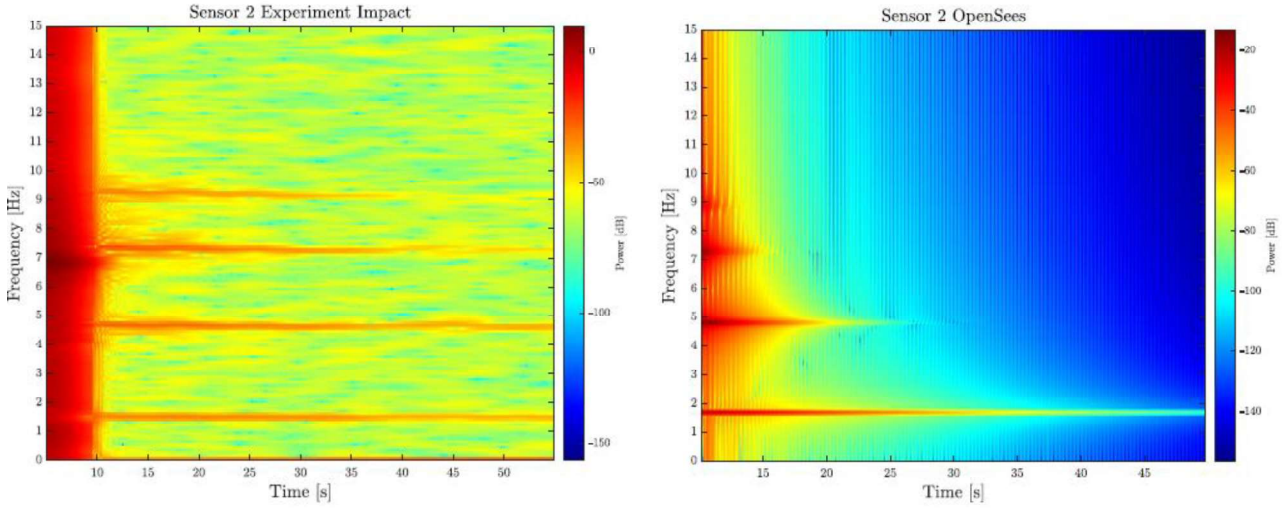

Fig. 4 – Spectrograms of impact loading obtained from experimental data (left) and FEM modelling (right)

The main four modes of the four-storey structure can be clearly identified from both spectrograms of Fig. 4. The impact effects are also evident (red region at the beginning) from these plots. The structural frequencies were also clearly identifiable from similar plots constructed on the basis of ambient vibrations. These values were also verified with power spectral density plots and Stochastic System Identification (SSI) techniques. In general, the experimental frequencies are encouragingly close to the FEM frequencies with average errors of 2.6% for the unloaded and 1.9% for the loaded structure.

4. Damage identification

The results presented in the previous section correspond to the undamaged structure. In order to test the ability of the low-cost vibration sensing equipment to track progressive states of damage, three damage states were considered as follows (see Fig. 5):
Stage 1: The two bolts at the beam-column connections of levels 2 and 3 are loosened to 15% of their initial torque.
Stage 2: The beam depths are reduced by 80% starting at level 2 and progressing to levels 1 and 3.
Stage 3: The column sections at both ends of the ground storey are reduced to 10% of their original value.

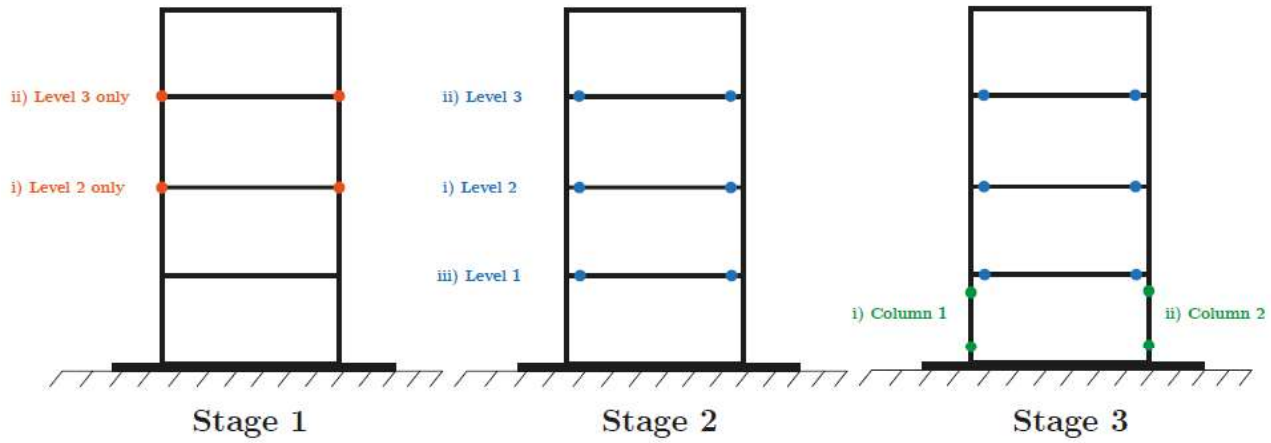

Fig. 5 – Damage states considered

As expected, the natural frequencies drop with increasing damage for all scenarios. However, there are discrepancies between each mode. For Stage 1, Mode 2 and Mode 3 show the highest absolute drops with up to 1.04 Hz for Mode 2 the FEM and an average of 0.81 Hz for Mode 3 in the experiment. Mode 4 is less influenced by the damage, with the largest drops of 0.06 Hz for Stage 3 in the FEM and 0.23 Hz experimentally. It should be recalled that the lower modes are also more dominant in the context of the SSI calculations as they vibrate longer than the highest one. In Stage 2 and Stage 3, Mode 2 reduces the most with a maximum overall drop of 0.72 Hz in the FEM and an average drop of 0.8 Hz experimentally. While it is not noticeable in the FEM, it was obvious from the experimental data in that the damage of columns produced a significant drop in frequencies, especially for modes 2 and 3.

Fig. 6 presents the evolutions of the structural frequencies for the 4 main modes of the frame at different damage states. As expected, the frequency change corresponding to the second mode experiences larger changes due to the pattern of the damage simulated (see Fig. 5). Also, the damping ratio of the first mode (as calculated from the FEM) is observed to increase for more severe damage states. A very good comparison between the numerical and experimentally obtained frequencies is observed.

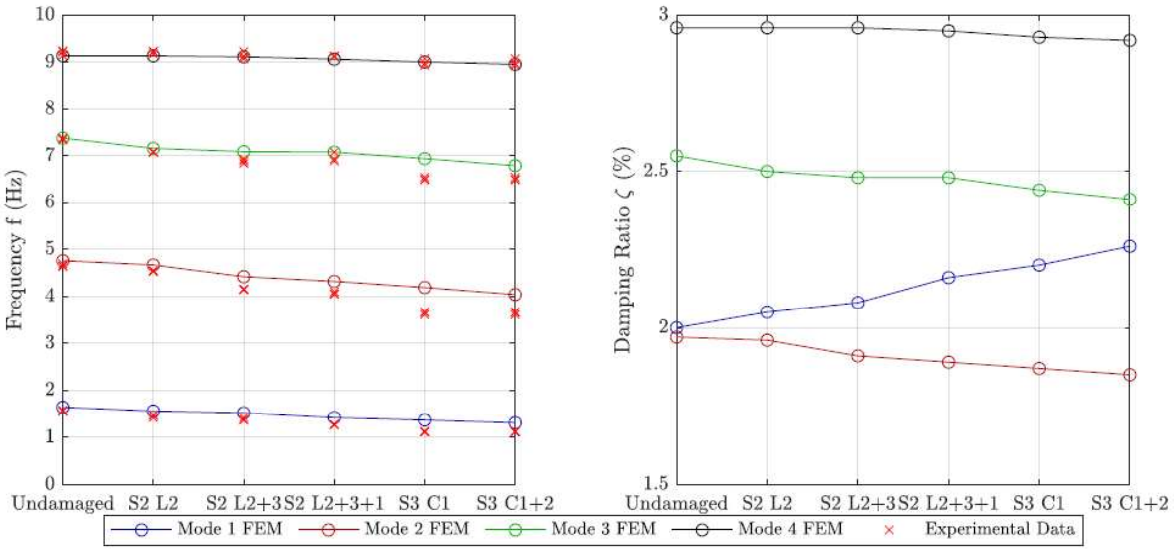

Fig. 6 – Evolution of structural frequencies at damage states 2 and 3

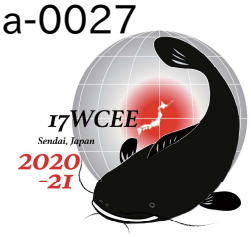

5. Evolution of the damping matrices

The identification of structural damping is a complex issue because the state variables relevant to its determination are not always obvious. To start with, the widely employed Rayleigh's assumption that relates damping only to instantaneous generalized velocities is incomplete and, in fact, any model that guarantees non-negative energy dissipation can possibly represent damping. Roughly, damping is categorized into three classes [12]: i) material damping, ii) boundary damping, and iii) viscous damping. Therefore, the viscous damping matrix C and the hysteretic damping matrix D, which comprises both the intrinsic material and boundary damping, are differentiated in this work. Mathematically, viscous damping is proportional to velocity and hysteretic damping proportional to the magnitude of displacement [13]. Physically, viscous damping occurs from molecules rubbing against each other in a viscous fluid, which causes a resistive friction force. Structural damping can also be interpreted as a sliding friction mechanism between molecular layers in a material. Here, the friction force is proportional to the displacement from a rest position [13].

The identification of the damping matrix for the model structure under study was achieved using two different methods: Operational Modal Analysis (OMA) and Experimental Modal Identification (EMA). In particular, the methodologies proposed by Bajrić-Hodzić and Høgsberg [14] and Lee and Kim [15] are employed.

5.1 OMA method

The OMA method described in [14] is based on Lancaster's estimation. In this method, the mass distribution of the structure is assumed to be know or well estimated and where the damping matrix is defined as:

$$\boldsymbol{C} = -\boldsymbol{M}(\boldsymbol{\Phi}\boldsymbol{\Lambda}^2\boldsymbol{\Phi}^T + \bar{\boldsymbol{\Phi}}\bar{\boldsymbol{\Lambda}}^2\boldsymbol{\Phi}^H)\boldsymbol{M} \tag{1}$$

where H denotes the Hermitian transpose. Besides, complex modes are normalized so that:

$$\boldsymbol{\Phi}_i^T(2\lambda_i\boldsymbol{M} + \boldsymbol{C})\phi_i = 1, \text{with } i = 1, \dots, 2N \tag{2}$$

where N is the number of degrees of freedom. Therefore, the dynamic state matrix is [14]:

$$\boldsymbol{A} = \begin{bmatrix} \boldsymbol{0} & \boldsymbol{I} \\ (\boldsymbol{\Phi}\boldsymbol{\Lambda}^2\boldsymbol{\Phi}^{-1}(\boldsymbol{I} + \bar{\boldsymbol{\Phi}}\boldsymbol{S}\boldsymbol{\Lambda}\boldsymbol{\Phi}^{-1}) - \bar{\boldsymbol{\Phi}}\bar{\boldsymbol{\Lambda}}^2\boldsymbol{\Phi}^{-1}) & (\bar{\boldsymbol{\Phi}}\bar{\boldsymbol{\Lambda}}^2 - \boldsymbol{\Phi}\boldsymbol{\Lambda}^2\boldsymbol{\Phi}^{-1}\bar{\boldsymbol{\Phi}})\boldsymbol{S} \end{bmatrix} \tag{3}$$

Where the matrices $\boldsymbol{S} = (\bar{\boldsymbol{\Phi}}\bar{\boldsymbol{\Lambda}} - \boldsymbol{\Phi}\boldsymbol{\Lambda}\boldsymbol{\Phi}^{-1}\bar{\boldsymbol{\Phi}})^{-1}$ and $\boldsymbol{\Phi}$ are both non-singular. Finally, the damping matrix can be expressed as:

$$\boldsymbol{C} = \boldsymbol{M}(\boldsymbol{\Phi}\boldsymbol{\Lambda}^2\boldsymbol{\Phi}^{+1}\bar{\boldsymbol{\Phi}}\bar{\boldsymbol{\Lambda}}^2)\mathbf{S} \tag{4}$$

5.2 EMA method

The starting point of the method by Lee and Kim [15] is the equation of motion (EOM), which includes both the viscous damping matrix C and the hysteretic damping matrix D:

$$(\boldsymbol{K} - \boldsymbol{M}\omega^2) + j(\omega\boldsymbol{C} + \boldsymbol{D})\boldsymbol{X}(\omega) = \boldsymbol{F}e^{j\omega t} \tag{5}$$

where the displacement is $q(t) = \boldsymbol{X}(\omega)e^{j\omega t}$ and the system damping matrices can be obtained by means of a pseudo-inverse procedure as:

$$\begin{bmatrix} \boldsymbol{C} \\ \boldsymbol{D} \end{bmatrix}_{2nxn} = \begin{bmatrix} \boldsymbol{I} & \omega_1 \boldsymbol{I} \\ \boldsymbol{I} & \omega_1 \boldsymbol{I} \\ \vdots & \vdots \\ \boldsymbol{I} & \omega_k \boldsymbol{I} \end{bmatrix}_{knx2n} \begin{bmatrix} \Im(\boldsymbol{H}^{\boldsymbol{C}}(\omega_1)^{-1}) \\ \Im(\boldsymbol{H}^{\boldsymbol{C}}(\omega_2)^{-1}) \\ \vdots \\ \Im(\boldsymbol{H}^{\boldsymbol{C}}(\omega_k)^{-1}) \end{bmatrix} \tag{6}$$

5.3 Damping matrix evolution from OMA

In damage state 1, the highest damping ratio reduction was observed at levels 1, 2 and 4 with 5.8%, 4.6% and 6.1% reductions for the bolt loosening at Level 2 and 2.9 %, 6.7% and 7.1% reduction for the bolt loosening at Level 3, respectively. In the case of damage state 2, presented in Fig. 7 below, the damping coefficients ξ_{33} and ξ_{11} are reduced by 1.2% and 1.3% while ξ_{22} does not reduce at all. The damage in state 3 includes the section reduction of the columns below Level 1 (as well as the beam reduction already effecting from state 2. Therefore, a significant change in damping coefficients was expected. This was clearly observed with the first column reduction causing a further drop from 1.2 % to 4.6 % of ξ_{11} and the second column reduction a drop of 22.1% at Level 1. The drop of the other stiffness coefficients are more or less negligible, except for ξ_{12} and ξ_{21} where an overall drop of 3.1% was observed.

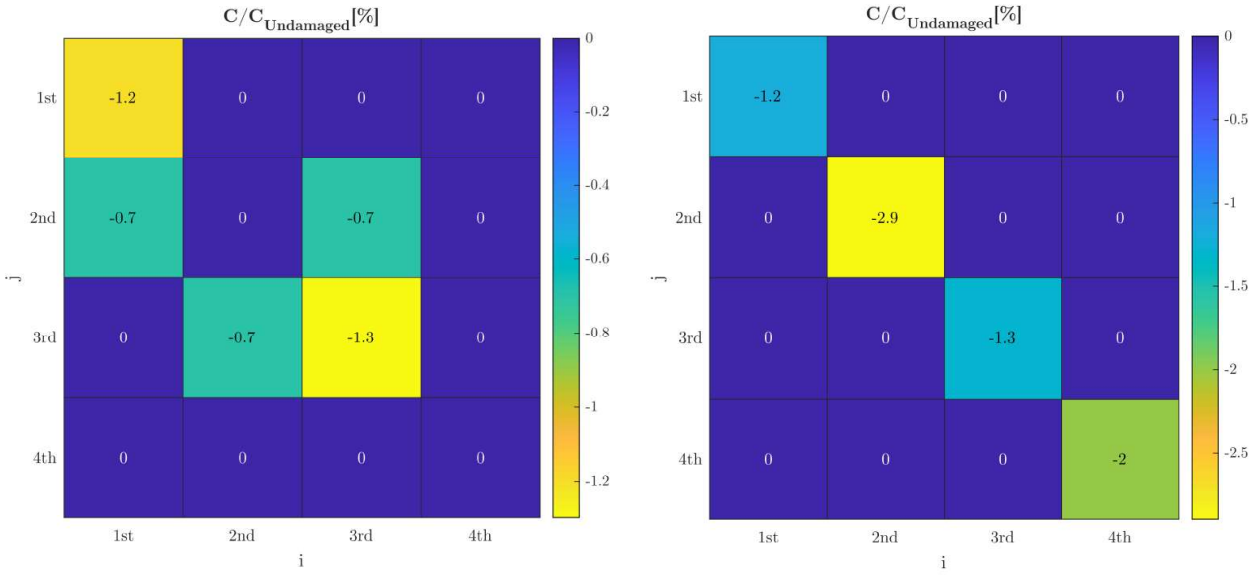

Fig. 7 – Percentage reduction in damping on the Damping Matrix **C** at damage state 2 affecting Level 2 only (left) and Levels 1 to 3 (right) as obtained from OMA

5.4 Damping matrix evolution from EMA

For the viscous damping matrix **C**, we can see the same reduction of diagonal damping coefficients above and below the level of damage as previously observed when the OMA method was applied. For damage state 1, these drops are slightly higher, with maximum drops of 8.18% and 12.29 % for ξ_{33} for Level 2 and ξ_{44} for Level 3, respectively. Damage stage 2 causes a maximum drop of 2.87% for ξ_{22} for section reductions at Level 1, 2 and 3, which matches well with the OMA results. These latter results are summarized in Fig. 8 which presents the damping matrices C obtained with EMA. As before, the largest change was observed when the columns were affected in state 3. In general, the evolution of the **C** matrix is consistent with the observations from the OMA method.

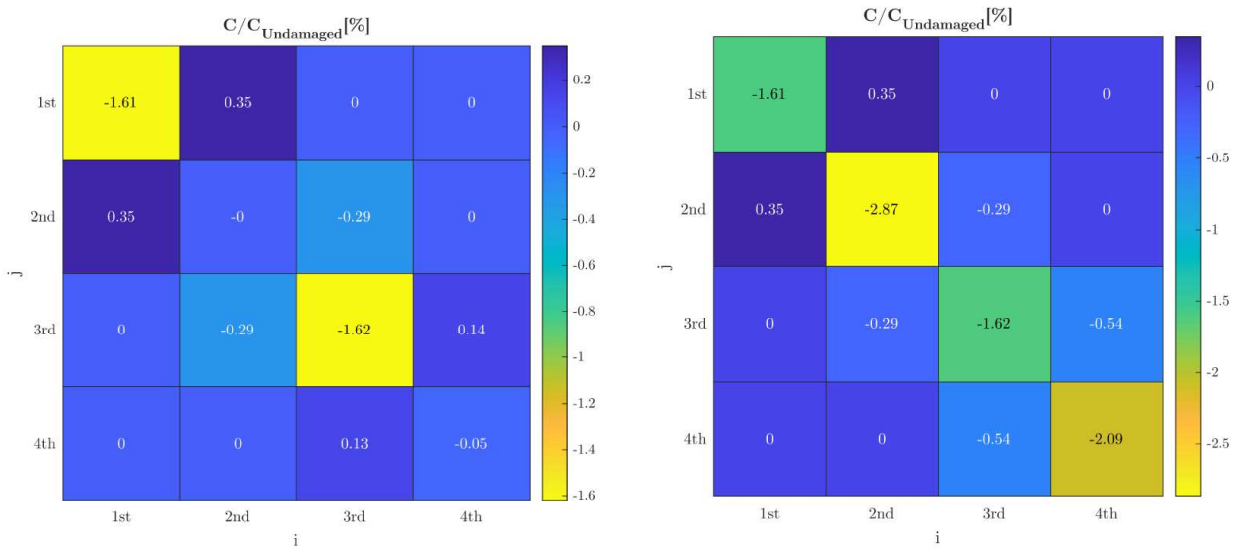

Fig. 8 – Percentage reduction in damping on the Damping Matrix **C** at damage state 2 affecting Level 2 only (left) and Levels 1 to 3 (right) as obtained from EMA

The hysteretic damping matrix **D** shows a similar evolution at different damage states and elements affected as that already discussed for matrix **C**. The main difference is related to the off-diagonal terms that are affected with more or less the same magnitudes as the diagonal terms in this case. For state 1, the largest overall drop occurs for ξ_{22} with 7.18 % while ξ_{44} with a drop of 3.61 % is much less affected than in the case of the viscous damping matrix. For damage state 2, which results are presented in Fig. 9, the evolution of hysteretic damping shows more differences with respect to the viscous damping matrix. In this case, the hysteretic damping change affects the terms corresponding to the level affected. At Level 2 for example, one can see that a drop of 1.72% in ξ_{22} larger than the other diagonal terms. The largest overall drop occurs for ξ_{33} (3.68 %).

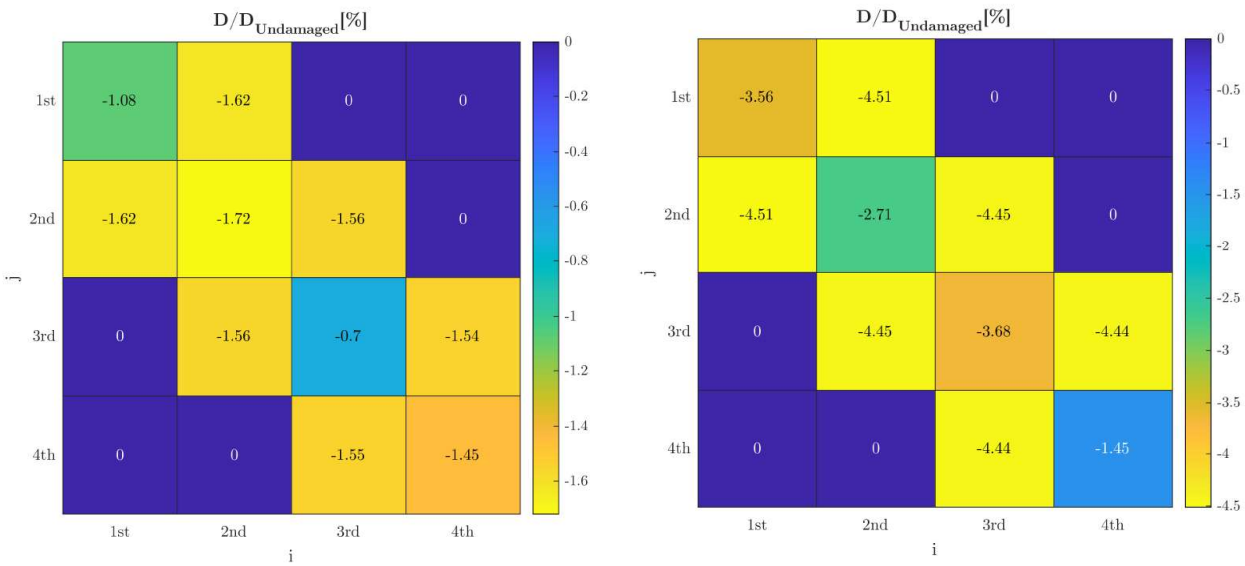

Fig. 9 – Percentage reduction in damping on the Damping Matrix **D** at damage state 2 affecting Level 2 only (left) and Levels 1 to 3 (right) as obtained from EMA

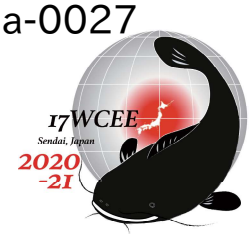

6. Evolution of the stiffness matrices

The focus of this paper is on the damping identification. This is because damping quantification represents an important challenge for experimental dynamics and hence constitutes a good limit test for the capabilities of the wireless low-cost sensing system proposed in this study. However, stiffness computations are also presented in this section for completeness.

Fig.10 presents the percentage change in stiffness between the un-damaged state and damage state 2 obtained from the OMA and EMA methodologies described above. It can be observed in this figure that for the OMA case, a loss of 4.3 % in k_{11} and k_{33}, and a maximum of 8.7 for k_{44}, for damage state 2 affecting the beams at storeys 1 to 3. The pattern of change in the stiffness coefficients is similar to that previously observed for damping. However, it is interesting to see that the change of all other stiffness coefficients is barely noticeable. It is also worth noting that the largest stiffness drop is observed for damage state 3, when the columns at the ground level are affected and k_{11} drops by 22.1 %. It is also worth mentioning that both the EMA and OMA methods lead to almost identical values of stiffness matrix change. This is clearly different from the results for damping matrices presented above, where both methods showed similar patterns but noticeable discrepancies in magnitude. This is an encouraging result that not only evidences consistency in results but gives confidence to the use of low-cost vibration-based monitoring for coarse damage localization.

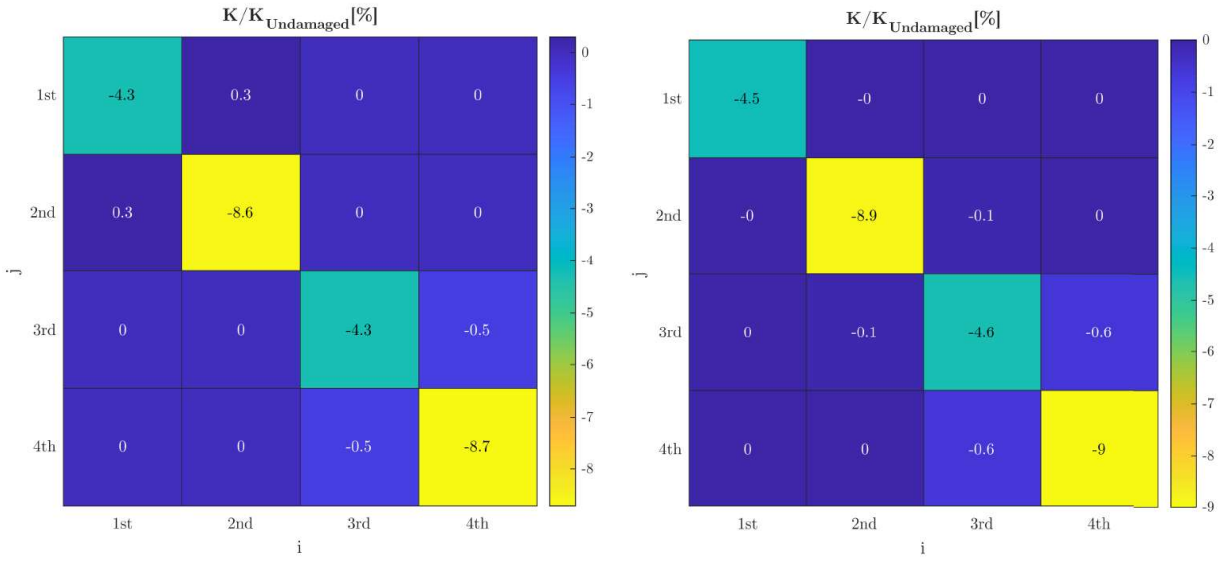

Fig. 10 – Percentage reduction in stiffness on the Stiffness Matrix **K** at damage state 2 affecting levels 2 to 3 obtained from OMA (left) and EMA (right)

7. Conclusions

This paper has examined the use of low-cost wireless acceleration sensors for structural characterization, damage identification and coarse damage localization. Over the last decades, multiple studies proposing the use of low-cost off-the-shelf MEMS accelerometers have been carried out. This speaks to the accessibility and ease with which microcontrollers and MEMS can be assembled and tested to construct accelerographs and sensing units with various configurations being published regularly in the technical and non-technical literature [1-6]. A wireless sensing network based on such open-electronic components was proposed and used in this study.

Recognising that a proper experimental characterization of structural damping is one of the most current and challenging topics in mechanics, the experimental formulation of damping matrices was chosen as a test for the ability of low-cost accelerometers to retrieve useful information in the context of damage identification. To this end, a series of tests were conducted on a model structure representing a 4-storey frame. The structure

was subjected to successive stages of damage by means of section reduction and bolt loosening and the acceleration records were employed to extract stiffness and damping matrices through Operational Modal Analysis (OMA) and Experimental Modal Identification (EMA) procedures.

The practical choice between the OMA and the EMA methods will depend on the scale of the structure and the given budget. The output-only OMA method employed has the great benefit of not requiring knowledge of the type or magnitude of the external action and is particularly suited for structures that are subjected to unknown excitations. The results obtained from OMA for the stiffness and damping matrices show a good overall accuracy in comparison with numerical simulations, as long as stable estimates of modal shapes and damping ratios can be obtained from the data collected. One major drawback of this method, however, is the sensitivity of the results to noisy data. Although stable poles are found, the SSI algorithm employed struggled to estimate modal shapes and damping ratios sometimes leading to unphysical results. This is exacerbated if acceleration histories need to be integrated and the choice of filter becomes a key consideration. Besides, the high level of user involvement, the OMA method employed only outputs viscous damping matrices.

The experimental modal analysis (EMA) method employed here, on the other hand is most suitable when the input force is known at each DOF. It showed a high level of accuracy and required much less user interaction as stability criteria and number of poles are not included in the inputs. The fact that this method operates in the frequency domain also relaxes significantly the requirements of data synchronization of the low-cost sensors. In addition, the EMA method used in this paper also calculates the hysteretic damping matrix (**D**) which is easier to relate physically to the damage evolution in the structure being studied.

The localisation of damage is an important aspect of post-earthquake structural assessments since it allows the inspector to separate structurally healthy from unhealthy structures. Since damage localization is not possible based only on frequency changes, this paper has also sought to explore the use of changes in damping and stiffness matrices generated from low-cost vibration data. This can be difficulted by the sensitivity to pole identification mentioned before but the results presented in this paper indicate that once the damping matrix is successfully generated, a localisation is indeed possible. It was observed that both OMA and EMA methods lead to similar evolutions in the variations of the damping and stiffness matrices. For example, a damaged beam consistently causes a reduction in damping above and below that level, both in its viscous and the hysteretic damping formulations. These or similar patterns can be used to inform more detailed structural inspections. Besides, the use of stiffness matrices also provides stable estimates of probable damage and both (stiffness and damping) matrices can be used in conjunction to increase the level of confidence on the structural evaluations performed.

6. References

[1] Lee-Lewis T, Málaga-Chuquitaype C, Nanos N (2019): On the use of low-cost vibration sensing technologies for seismic assessment in urban areas. *SECED Conference 2019, Earthquake Risk and Engineering Towards a Resilient World*, London, UK.

[2] Bedon C, Bergamo E, Izzi M, Noè S (2018). Prototyping and Validation of MEMS Accelerometers for Structural Health Monitoring—The Case Study of the Pietratagliata Cable-Stayed Bridge. *Journal of Sensor and Actuator Networks*, 7(3), 30.

[3] Sabato A, Niezrecki C, Fortino G (2017): Wireless MEMS-Based Accelerometer Sensor Boards for Structural Vibration Monitoring: A Review. *IEEE Sensors Journal*, 17(2), 226–235.

[4] Varanis M, Silva AL, Mereles AG (2017): On mechanical vibration analysis of a multi degree of freedom system based on arduino and MEMS accelerometers. *Revista Brasileira de Ensino de Física*, 40(1), 1–11.

[5] Hummel H (2020): Structural Assessment and Spatial Damping Identification, *MSc Dissertation*, Imperial College London, UK.

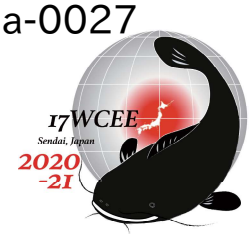

[6] Evans JR, Allen RM, Chung AI, Cochran ES, Guy R, Hellweg M, Lawrence JF (2014): Performance of Several Low-Cost Accelerometers. *Seismological Research Letters,* 85 (1). pp. 147-158. ISSN 0895-0695.

[7] Chen HP (2018): Structural Health Monitoring of Large Civil Engineering Structures. Wiley Blackwell.

[8] Hanly S (2020): Top 9 accurate wireless vibration monitoring systems. https://blog.endaq.com/top-accurate-wireless-vibration-monitoring-systems#WSeries.

[9] enDAQ Sensors (2020): Shock, vibration & environmental sensors. https://endaq.com/collections/endaq-sensors-shock-vibration-s-series.

[10] Bajric-Hodzic A (2017): Identification of damping from structural vibrations. *PhD thesis*, Department of Mechanical Engineering, Technical University of Denmark.

[11] McKenna F (1997): Object oriented finite element analysis: Frameworks for analysis algorithms and parallel computing. *PhD dissertation*, University of California, Berkeley.

[12] Arora V (2014): Direct structural damping identification method using complex frfs. *Journal of Sound and Vibration*, 51: 133-143.

[13] Richardson M, PotterR (1975):Viscous vs. structural damping in modal analysis. 46th *Shock and Vibration Symposium*.

[14] Bajrić A, Høgsberg J (2017): Identification of damping and complex modes in structural vibrations. *Journal of Sound and Vibration*, 431:367–389.

[15] Lee JH, Kim J(2001): Development and validation of a new experimental method to identify damping matrices of a dynamic system. Journal of Sound and Vibration, 246: 505-524.

